Room-Temperature Antiferromagnetic Resonance and Inverse Spin-Hall Voltage in Canted Antiferromagnets

I. Boventer,[1] H. T. Simensen,[2] A. Anane,[1] M. Kläui,[2,3,4] A. Brataas,[2] and R. Lebrun[1,*]
[1]Unité Mixte de Physique, CNRS, Thales, Université Paris-Saclay, 91767, Palaiseau, France
[2]Center for Quantum Spintronics, Department of Physics, Norwegian University of Science and Technology, Trondheim NO-7491, Norway
[3]Institut für Physik, Johannes Gutenberg-Universität Mainz, D-55099 Mainz, Germany
[4]Graduate School of Excellence Materials Science in Mainz (MAINZ), Staudingerweg 9, D-55128 Mainz, Germany

(Received 13 November 2020; accepted 30 March 2021; published 6 May 2021)

We study theoretically and experimentally the spin pumping signals induced by the resonance of canted antiferromagnets with Dzyaloshinskii-Moriya interaction and demonstrate that they can generate easily observable inverse spin-Hall voltages. Using a bilayer of hematite/heavy metal as a model system, we measure at room temperature the antiferromagnetic resonance and an associated inverse spin-Hall voltage, as large as in collinear antiferromagnets. As expected for coherent spin pumping, we observe that the sign of the inverse spin-Hall voltage provides direct information about the mode handedness as deduced by comparing hematite, chromium oxide and the ferrimagnet yttrium-iron garnet. Our results open new means to generate and detect spin currents at terahertz frequencies by functionalizing antiferromagnets with low damping and canted moments.

DOI: 10.1103/PhysRevLett.126.187201

Contemporary spintronics, utilizing the electronic spin for information processing and microelectronics, is mostly based on ferromagnetic device architectures. In view of long-term perspectives to enable enhanced data processing speeds and downscaling for on-chip information processing [1], spintronics with antiferromagnets is a promising avenue [2]. Antiferromagnets exhibit the key advantage over ferromagnets that their resonance frequency is enhanced by the exchange coupling of the sublattices, and thus generally in the terahertz regime [2,3]. In compensated antiferromagnets, the absence of a net moment however strongly impedes simple access to their ultrafast dynamics, especially in thin films, and the development of ultrafast antiferromagnet-based devices [4,5]. As a result, interfacial spin-transport phenomena could provide new insights into the spin-relaxation processes and spin dynamics in antiferromagnets [5–8].

Experimental access to the spin dynamics can be facilitated by spin to charge conversion mechanisms such as the spin pumping effect largely studied in ferromagnets [9,10]. The spin pumping effect generates alternating (ac) and continuous (dc) spin currents from the spin precession of a magnetic material into an adjacent conductor [11,12]. These spin currents can be detected electrically by measuring a voltage via the inverse spin-Hall effect (ISHE) [12] or through the inverse Rashba-Edelstein effect [13]. Applied to antiferromagnets (AFMs), these combined spintronic effects could provide a direct and surface sensitive access to the magnetization dynamics in both bulk and thin AFM films. However, theoretical [14,15] and recent experimental studies [16,17] showed that, in collinear antiferromagnets, the amplitude of the pumped spin currents scales with the dynamical sublattice symmetry breaking. Thus, its amplitude is proportional to the ratio of the anisotropy field H_A and the exchange field H_E. This ratio is of less than 0.1% in many compounds [5,6,15], and only reaches 1%–2% in two known compounds MnF_2 [18] and FeF_2 [19] without applying large magnetic fields of the order of the spin-flop field. This limitation has until now largely restrained the investigation of spin-pumping signals in antiferromagnets.

In parallel, routes to generate spin-pumping signals from noncollinear antiferromagnets have not been widely considered yet. Early studies have reported that the bulk Dzyaloshinskii Moriya interaction (DMI) can reach a few teslas in some antiferromagnets, and induce small canted moments both for easy axis (e.g., NiF_2 [20], CoF_2 [20] or most orthoferrites [21,22]) and easy-plane antiferromagnets (e.g., $MnCO_3$ [20] or hematite, α-Fe_2O_3, above the Morin transition [23]), or chiral antiferromagnets (e.g., Mn_3Sn [24]).

In this Letter, we explore both theoretically and experimentally spin pumping in noncollinear antiferromagnets with a DMI induced canting and capped with a heavy metal. First, we demonstrate theoretically that the AFM resonance generates a dc spin pumping and an inverse spin-Hall voltage V_{ISHE} in the adjacent heavy metal, proportional to the ratio H_D/H_E (H_D: DMI field, H_E: exchange field). This result is valid in both easy-axis and easy-plane canted AFMs. Note, that the zero-field mode frequencies

do not depend directly on the DMI field. We anticipate inverse spin-Hall voltages $V_{\mathrm{ISHE}} > 100$ nV in many canted AFMs with $H_D/H_E \propto 1\%$–10% [23,25]. In parallel, their zero-field mode frequencies can range from tens to hundreds of gigahertz (depending on the exchange H_E and anisotropy H_A fields of the materials [23,25]). Second, we experimentally study hematite (α-Fe_2O_3) capped with platinum to confirm our theoretical predictions. Because of the low Gilbert damping and its residual anisotropy in the easy-plane phase [23,26,27], we easily measure the resonance of the low frequency mode f_- of hematite [6,23,28,29] and its associated V_{ISHE}. We report $V_{\mathrm{ISHE}} > 30$ nV at 300 K as large as in the uniaxial antiferromagnet chromium oxide (Cr_2O_3) at low temperatures and only one order of magnitude smaller than in the ferrimagnetic insulator YIG. Furthermore, a direct comparison between the signs of the V_{ISHE} in the three compounds allows an identification of their respective mode handedness. Altogether, our results highlight that canted antiferromagnets embrace the rich dynamics of antiferromagnets, whilst keeping a net moment as in ferromagnets, and a larger temperature stability than ferrimagnets with compensated angular momentum [30].

We start by deriving theoretically the spin-pumping response associated with the magnetization dynamics of both canted easy-axis and easy-plane antiferromagnets when put in contact with normal metals. To this end, we model the magnetization dynamics in a macrospin approximation with two sublattices. We include the contributions from a DMI field $\boldsymbol{H}_D$ and an external magnetic field $\boldsymbol{H}$ orthogonal to the Néel order parameter. Both these fields contribute to the canted moments and, hence, to the emergence of a finite magnetic moment. The system's free energy reads

$$F = M\Big[H_E(\boldsymbol{m}_A\cdot\boldsymbol{m}_B) - H_D\hat{\boldsymbol{z}}\cdot(\boldsymbol{m}_A\times\boldsymbol{m}_B) + \frac{H_A}{2}(m_{A,z}^2+m_{B,z}^2) - \frac{H_a}{2}(m_{A,y}^2+m_{B,y}^2) - \boldsymbol{H}\cdot(\boldsymbol{m}_A+\boldsymbol{m}_B)\Big], \quad (1)$$

where γ denotes the gyromagnetic ratio, $\boldsymbol{m}_i$ the unit vector of the sublattice magnetization $\boldsymbol{M}_i$ ($i\in\{A,B\}$), $\boldsymbol{M}_i = M\boldsymbol{m}_i$, and $\boldsymbol{H} = H\hat{\boldsymbol{x}}$ is the externally applied static magnetic field, H_A denotes the hard-axis anisotropy along the z axis, and H_a the easy-axis anisotropy within the xy plane. The above model can be applied on both canted easy-axis ($H_A = 0$) and canted easy-plane ($H_A \gg H_a$) AFMs. In these AFMs, the eigenmodes are nondegenerate with a low frequency mode f_- and a high frequency mode f_+:

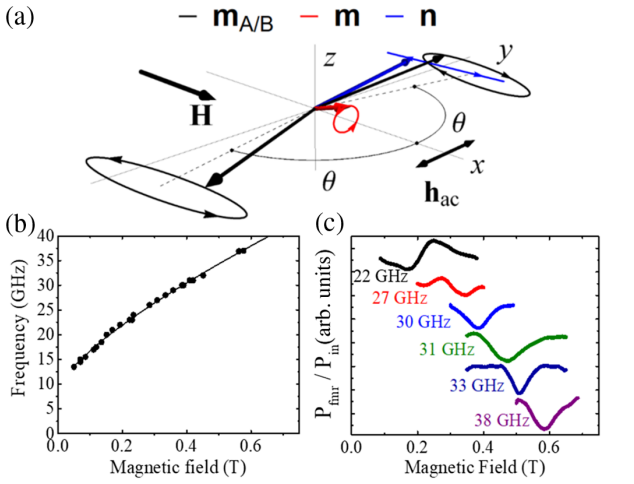

FIG. 1. Magnetic resonance of the low frequency mode of hematite. (a) Illustration of the low frequency mode of hematite in the easy-plane phase in presence of a DMI induced canting. (b) The frequency dispersion of the low frequency mode of hematite measured from 10 to 40 GHz. Using Eq. (2), we extract the parameters for the anisotropy field $H_a = 6\times10^{-5}$ T and the DMI field $H_D = 2.26$ T. (c) Resonance curves for different values of the externally applied field. The data are normalized by the input power.

$$f_- = \left(\frac{\gamma}{2\pi}\right)\sqrt{2H_EH_a + H(H+H_D)}, \quad (2)$$

$$f_+ = \left(\frac{\gamma}{2\pi}\right)\sqrt{2H_E(H_a+H_A) + H_D(H+H_D)}. \quad (3)$$

The eigenmodes are qualitatively similar in canted easy-plane and canted easy-axis AFMs (see Supplemental Material [31]). Hence, we can continue with a generalized model that describes both systems. This contrasts with the collinear easy-axis and easy-plane AFMs, in which the modes are profoundly different and need separate treatments [14–17,33,34]. The low frequency mode of canted AFMs is characterized by a right-handed elliptical precession of the magnetic moment [see Fig. 1(a)]. The high frequency mode is characterized by a linearly oscillating magnetization (see Supplemental Material [31]). Note that, in the absence of an applied field, the gap of the low frequency mode [Eq. (2)] depends only on the exchange H_E and easy-axis anisotropy H_a, and not on the DMI field H_D. This remarkable feature causes a low frequency mode in the THz range in canted easy-axis AFMs such as $ErFeO_3$ [35]. In canted easy-plane AFMs where H_a is often much smaller, the low frequency mode can even be found in the range of a few GHz, such as for hematite above the Morin temperature [23].

We next derive an expression for the inverse spin Hall voltage V_{ISHE} induced by spin pumping from the low frequency mode into an adjacent heavy metal layer. We consider excitations by an oscillating magnetic field $\boldsymbol{h}_{\mathrm{ac}}$

(applied along the $\boldsymbol{y}$ axis) at the resonance frequency f_-, which induces the precession of the magnetic moments within the (yz) plane. The transverse V_{ISHE} voltage (along $\boldsymbol{y}$) is proportional to the dynamic magnetization amplitudes in both the y and z directions. Following the approach of Ref. [14], we establish the expression for the inverse spin-Hall voltage V_{ISHE} (see Supplemental Material [31] for details):

$$V_{\mathrm{ISHE}} = \frac{\hbar\theta_{\mathrm{SH}}}{8}\frac{d_V}{d_N}\gamma^3\left(\frac{h_{\mathrm{ac}}}{H_E}\right)^2 Q^2\frac{(H+H_D)^3}{4\pi^2 f_-^2} \times \frac{\lambda e G_R \tanh(d_N/2\lambda)}{h\sigma + 2\lambda e^2 G_R \coth(d_N/\lambda)}, \quad (4)$$

where G_R denotes the real part of the spin mixing conductance per unit area of the interface, h_{ac} is the amplitude of the excitation field, e is the elementary charge, d_V is the distance between the voltage leads, d_N is the Pt layer's thickness, θ_N, λ, and σ are the thickness, spin diffusion length, and the conductivity of Pt, respectively. $Q_- = f_-/\Delta f_-$ corresponds to the material quality factor with $\Delta f_- = \alpha(\gamma/\pi)H_E$ the linewidth of the low frequency resonance peak [28]. The expression of the antiferromagnetic linewidth and the damping values remain under strong debate in antiferromagnets [23,28,36,37]. However, resonance measurements in insulating antiferromagnets generally show Q_- factors in the range of 100–1000 [38–42]. We thus chose to evaluate the expected inverse spin-Hall voltages V_{ISHE} for prototypical canted antiferromagnets such as orthoferrites with Q_- factors of 500, in the range of the existing reports [38,41,42], and note that it can reach 0.5 μV (for $h_{\mathrm{ac}} = 1$ mT, i.e., one tenth of the ac field used in Ref. [16]). For a given Q_- factor, V_{ISHE} scales with $(H+H_D)^3/H_E^2 f_-^2$. As f_- scales with H, we anticipate a linear increase of the inverse spin-Hall voltage V_{ISHE} with the applied field (for $H \gg H_D$) which is opposite to the ferromagnetic case [43].

The predicted inverse spin-Hall voltages presented in Table I are all above 10 nV which is in the accessible range of conventional voltage measurements [12,44]. Therefore, canted antiferromagnets with DMI induced canting open very promising perspectives for examining the electrical response of antiferromagnetic dynamics in the terahertz regime.

To confirm our predictions, we next experimentally investigate the antiferromagnetic resonance and the generated inverse-spin Hall voltage in 500 μm thick bulk crystals of hematite covered [26] by a 3 nm thick Pt layer. We then compare the recorded inverse spin Hall effect voltages to the ones of the ferrimagnet YIG and the easy-axis antiferromagnet Cr_2O_3 [17] to also obtain further information such as the mode handedness as expected for a coherent spin-pumping signal.

In the antiferromagnetic insulator hematite, the DMI field induces a small canted moment ($\sim$3 emu/cm^3) of the two sublattices above the Morin temperature ($T_M \sim 250$ K). For $T > T_M$, its magnetic configuration corresponds to a canted easy-plane phase with a residual in-plane anisotropy H_a such that it exhibits a low frequency mode in the gigahertz (GHz) range [23,28,29]. Therefore, we can conduct our measurements using a state-of-the-art highly sensitive wideband resonance spectrometer ($1-40$ GHz) with a broadband coplanar waveguide (cf. Supplemental Material, Fig. 1 [31]) and at room temperature. In Figs. 1(a)–1(c), we present the dynamics and the frequency dispersion of the low frequency mode of hematite which has a gap around 15 GHz in agreement with previous reports [23,28].

Correspondingly, we characterize the spin-pumping efficiency at the α-Fe_2O_3/Pt interface by measuring the voltage generated at resonance in the top platinum layer using a lock-in technique. This allows us to validate our model and investigate the spin dynamics of this non-collinear antiferromagnet. We measure a voltage peak at resonance only in the transverse configuration [see inset of Fig. 2(a)], and a clear sign reversal when we reverse the direction of the applied magnetic field. This sign inversion demonstrates the spin-pumping origin of the generated voltage. This result is to our knowledge the first evidence of spin pumping from an easy-plane antiferromagnet and, more generally, at room temperature for an antiferromagnet.

As for ferromagnets [12], we only measure a nonzero V_{ISHE} in the transverse configuration when the magnetic field is perpendicular to the voltage contacts as shown in Fig. 2(a). In this configuration, the dc spin accumulation $\boldsymbol{\sigma}$

TABLE I. Expected inverse spin Hall effect voltages V_{ISHE} with their leading quantities H_E, H_A, H_a, and H_D (taken at room temperature) for each of the listed canted antiferromagnets. All voltages are calculated with a material quality factor $Q_- = 500$ for the different materials, an excitation field $h_{\mathrm{ac}} = 1$ mT, an external field $H = 0.2$ T to ensure a monodomainization, and a distance between the voltage leads of 3 mm. G_R is set to 6×10^{18} m^{-2}, λ to 1.2 nm, θ_{SH} to 0.1 taken from Refs. [26,43,45].

Material	H_E (T)	H_A (T)	H_a (T)	H_D (T)	f_- (THz)	V_{ISHE} (nV)
α-Fe_2O_3 [23,26,28]	1000	2×10^{-3}	6×10^{-5}	2.26	0.022	200
$YFeO_3$ [46,47]	640	⋯	0.06	14	0.25	711
$ErFeO_3$ [48,49]	600	⋯	0.03	10	0.17	628
$TmFeO_3$ [35,50]	550	⋯	0.1	4	0.3	18

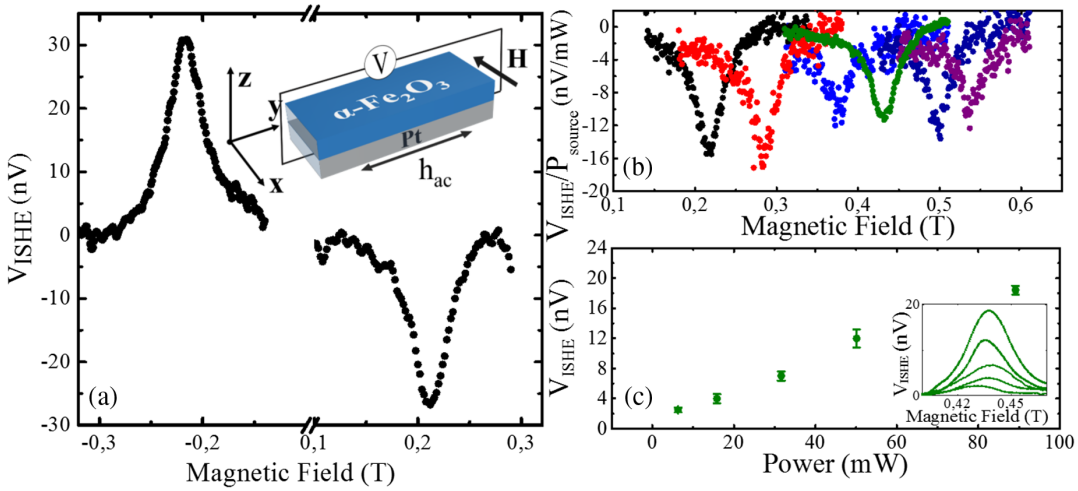

FIG. 2. Inverse spin Hall effect voltages V_{ISHE} in the easy-plane antiferromagnet hematite with a Dzyaloshinskii-Moriya interaction induced canted moment. (a) ISHE voltage measurement at ± 0.2 T in transverse configuration. (See inset for different signs of the external field H.) The antisymmetric signal shape indicates the recorded voltage to originate from spin-pumping. (b) V_{ISHE} for different frequencies as a function of the external magnetic field. Color coding of frequencies is consistent with Fig. 1(c). (c) Dependence of V_{ISHE} peak as a function of the applied microwave power for a fixed excitation frequency of 31 GHz. In the measured range, the ISHE voltage increases linearly as expected from Eq. (4). Inset shows the field dependency for the different powers.

generated at resonance must be parallel to the applied field and thus directed along the canted net moment in order to generate a nonzero charge current $\boldsymbol{J}_c \propto \boldsymbol{J}_S \times \boldsymbol{\sigma}$, leading to V_{ISHE}. This result seems at first contradictory to the spin-transport measurements in easy-plane antiferromagnets where pairs of propagating magnons carry spin-angular momentum along the direction of the antiferromagnet Néel order [29,51]. However, there is a key difference between the excitation processes. For the spin-transport case, the current induced spin accumulation generates pairs of correlated magnon modes with different wave vectors $\mathbf{k}$, leading to an effective nonzero spin-angular momentum along the Néel order. For the antiferromagnetic resonance case, the microwave magnetic field excites only uniform oscillations ($\mathbf{k} = 0$) which are linearly polarized in an easy-plane system. Thus, only the dynamics of the canted moment, induced by the external magnetic field $\mathbf{H}$ or the DMI field $\mathbf{H}_D$, can generate at resonance a nonzero dc spin accumulation and thus a dc inverse spin-Hall voltage. As shown in Fig. 2(c), we also observed a linear increase of V_{ISHE} with the input power, confirming that we are still in a linear regime of excitation.

Having detected the inverse spin-Hall voltage we need to determine the origin of the pumped spin current. This origin is a key point in a long-standing debate in ferro- and ferrimagnetic systems [52,53] and, more recently, also debated for antiferromagnets [16,17,54,55]. At resonance, oscillations of the excited mode [14,15] or incoherent contributions from thermal magnons (due to a resonance induced thermal gradient [56]) can both contribute to a spin-pumping signal. However, right (RH)- and left-handed (LH) circularly polarized modes carry opposite angular momentum and should thus result in inverse spin-Hall voltages with opposite signs [16,17]. Thus, one can obtain key information about the mode contributing to the spin-pumping signals by analyzing the sign of the inverse spin-Hall voltages.

Using broadband coplanar waveguides up to 40 GHz, we can only access the low frequency RH mode above the Morin transition, and the LH mode below the Morin transition (see Supplemental Material [31]). However, we did not detect any V_{ISHE} for the LH of hematite at all temperatures below the Morin transition (see Supplemental Material [31]). This observation is consistent with a coherent spin-pumping signal associated to the dynamical sublattice symmetry breaking [14], which is extremely small in the easy-axis phase of hematite ($H_A/H_E \approx 10^{-6}$). To analyze its V_{ISHE} sign, we thus measure under the same conditions the inverse spin-Hall voltages from the LH mode of the easy-axis antiferromagnet Cr_2O_3 [17] and the RH mode of the ferrimagnet YIG [44] (see Fig. 3). To detect the LH mode of Cr_2O_3, we perform measurements close to the spin-flop field to reduce the mode frequency below 40 GHz. We observe that the LH mode of Cr_2O_3 and the RH modes of α-Fe_2O_3 and YIG show inverse spin-Hall voltages with opposite signs as expected from a coherent spin-pumping model. In line with previous reports on Cr_2O_3 [17], the V_{ISHE} of the LH mode disappears at high temperature (see Supplemental Material [31]) which is an indication of its coherent origin. Furthermore, the RH modes of α-Fe_2O_3 and YIG generate inverse spin Hall voltages with opposite signs compared to the thermal spin-pumping contribution of the RH mode of Cr_2O_3 reported in Ref. [17]. Lastly, the inverse spin-Hall

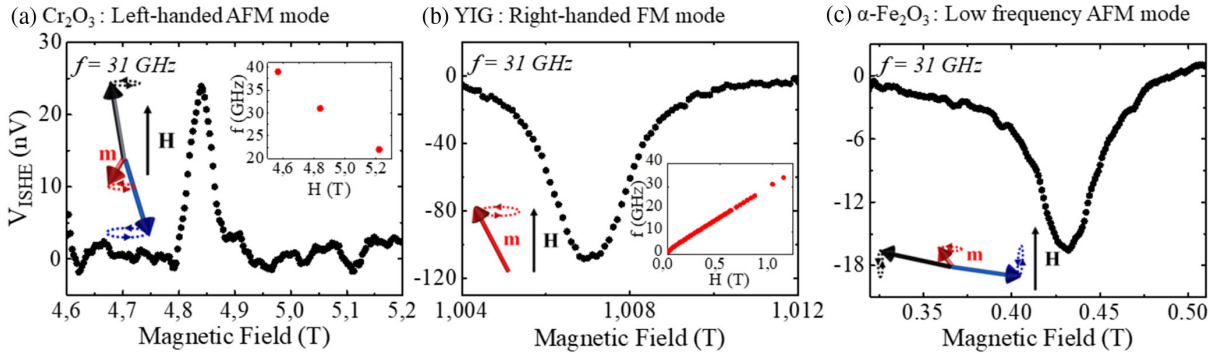

FIG. 3. Inverse spin-Hall voltages recorded at 31 GHz for (a) the left-handed AFM mode of the easy-axis antiferromagnet Cr_2O_3 (b) the right-handed FM mode for the ferrimagnet YIG and (c) the low frequency (right-handed) mode of the canted easy-plane antiferromagnet α-Fe_2O_3 capped with a platinum layer. For an inverse spin-Hall voltage originating from coherent spin pumping, a difference in handedness of the mode's polarization is expected which induces a change in the sign of V_{ISHE}. We confirm the correlation between the sign of the inverse spin-Hall voltage V_{ISHE} and the mode handedness since the sign changes from (a) to (b) and is equal from (b) to (c). Insets show the dispersion curves for the different modes. Illustrations show the orientation of the magnetic moments with respect to the external static field H. The thickness of the YIG film is 200 nm, and the two AFMs crystals are 500 μm thick. The measurements on YIG and α-Fe_2O_3 are performed at room temperature and the ones on Cr_2O_3 are performed at 30 K (see Supplemental Material [31]).

voltages have comparable amplitudes for the LH mode of the easy-axis AFM Cr_2O_3 and for the RH mode of the canted AFM α-Fe_2O_3, and are smaller than in YIG by less than an order of magnitude. This feature indicates that both collinear and noncollinear antiferromagnets can efficiently generate spin pumping while significantly enhancing the operating frequency of spintronic devices.

In summary, we theoretically and experimentally demonstrate that noncollinear antiferromagnets with DMI induced canting can generate sizable spin-pumping signals and associated inverse spin-Hall voltages. Using hematite as a room temperature model canted AFM, we measured a signal of $V_{ISHE} > 30$ nV for the low frequency right-handed mode confirming our theoretical predictions. By comparing with the right-handed mode of YIG and the left-handed mode of Cr_2O_3, we confirm that the mode handedness determines the sign of the inverse spin-Hall voltage. Consequently, canted antiferromagnets allow for accessing the spin dynamics of the hitherto almost unexplored spin dynamics of noncollinear antiferromagnets. Such extensions not only broaden the understanding of the physics of the spin dynamics and of the relaxation processes for various classes of antiferromagnets but also represent a step further toward the realization of terahertz applications based on antiferromagnetic spintronics.

R. L., A. A., and M. K. acknowledge financial support from the Horizon 2020 Framework Programme of the European Commission under FET-Open Grant Agreement No. 863155 (s-Nebula). M. K. acknowledges support from the Graduate School of Excellence Materials Science in Mainz (MAINZ) DFG 266, the DAAD (Spintronics network, Project No. 57334897). M. K. acknowledges support from the DFG Project No. 423441604 and additional support from SFB TRR 173 Spin +X (projects A01 and B02 No. 268565370). H. T. S., A. B., M. K. were supported by the Research Council of Norway through its Centres of Excellence funding scheme, Project No. 262633 "QuSpin."

*Corresponding author
romain.lebrun@cnrs-thales.fr

[1] B. Dieny *et al.*, Opportunities and challenges for spintronics in the microelectronics industry, Nat. Electron. Rev. **3**, 8 (2020).
[2] V. Baltz, A. Manchon, M. Tsoi, T. Moriyama, T. Ono, and Y. Tserkovnyak, Antiferromagnetic spintronics, Rev. Mod. Phys. **90**, 015005 (2018).
[3] O. Gomonay, V. Baltz, A. Brataas, and Y. Tserkovnyak, Antiferromagnetic spin textures and dynamics, Nat. Phys. **14**, 213 (2018).
[4] T. Kampfrath, A. Sell, G. Klatt, A. Pashkin, S. Mährlein, T. Dekorsy, M. Wolf, M. Fiebig, A. Leitenstorfer, and R. Huber, Coherent terahertz control of antiferromagnetic spin waves, Nat. Photonics **5**, 31 (2011).
[5] S. Foner, High-field antiferromagnetic resonance in Cr_2O_3, Phys. Rev. **130**, 183 (1963).
[6] P. R. Elliston and G. J. Troup, Some antiferromagnetic resonance measurements in α-Fe_2O_3, J. Phys. C **1**, 169 (1968).
[7] L. R. Maxwell and T. R. McGuire, Antiferromagnetic resonance, Rev. Mod. Phys. **25**, 279 (1953).
[8] C. Kittel, Theory of antiferromagnetic resonance, Phys. Rev. **82**, 565 (1951).
[9] M. V. Costache, M. Sladkov, S. M. Watts, C. H. van der Wal, and B. J. van Wees, Electrical Detection of Spin Pumping Due to the Precessing Magnetization of a Single Ferromagnet, Phys. Rev. Lett. **97**, 216603 (2006).

[10] Y. Tserkovnyak, A. Brataas, and G. E. W. Bauer, Spin pumping and magnetization dynamics in metallic multilayers, Phys. Rev. B **66**, 224403 (2002).

[11] M. Weiler, J. M. Shaw, H. T. Nembach, and T. J. Silva, Phase-Sensitive Detection of Spin Pumping via the ac Inverse Spin Hall Effect, Phys. Rev. Lett. **113**, 157204 (2014).

[12] E. Saitoh, M. Ueda, H. Miyajima, and G. Tatara, Conversion of spin current into charge current at room temperature: Inverse spin-Hall effect, Appl. Phys. Lett. **88**, 182509 (2006).

[13] J.-C. Rojas-Sánchez, S. Oyarzún, Y. Fu, A. Marty, C. Vergnaud, S. Gambarelli, L. Vila, M. Jamet, Y. Ohtsubo, A. Taleb-Ibrahimi, P. Le Fèvre, F. Bertran, N. Reyren, J.-M. George, and A. Fert, Spin to Charge Conversion at Room Temperature by Spin Pumping into a New Type of Topological Insulator: α-Sn Films, Phys. Rev. Lett. **116**, 096602 (2016).

[14] Ø. Johansen and A. Brataas, Spin pumping and inverse spin Hall voltages from dynamical antiferromagnets, Phys. Rev. B **95**, 220408(R) (2017).

[15] R. Cheng, J. Xiao, Q. Niu, and A. Brataas, Spin Pumping and Spin-Transfer Torques in Antiferromagnets, Phys. Rev. Lett. **113**, 057601 (2014).

[16] P. Vaidya, S. A. Morley, J. van Tol, Y. Liu, R. Cheng, A. Brataas, D. Ledermanand E. del Barco, Subterahertz spin pumping from an insulating antiferromagnet, Science **368**, 160 (2020).

[17] J. Li, C. B. Wilson, R. Cheng, M. Lohmann, M. Kavand, W. Yuan, M. Aldosary, N. Agladze, P. Wei, M. S. Sherwin, and J. Shi, Spin current from sub-terahertz-generated antiferromagnetic magnons, Nature (London) **578**, 7793 (2020).

[18] J. P. Kotthaus and V. Jaccarino, Antiferromagnetic-Resonance Linewidths in MnF_2, Phys. Rev. Lett. **28**, 1649 (1972).

[19] V. Jaccarino, A. R. King, M. Motokawa, T. Sakakibara, and M. Date, Temperature dependence of FeF_2 spin flop field, J. Magn. Magn. Mater. **31**, 1117 (1983).

[20] P. L. Richards, Antiferromagnetic resonance in CoF_2, NiF_2, and $MnCO_3$, J. Appl. Phys. **35**, 850 (1964).

[21] C. E. Johnson, L. A. Prelorendjo, and M. F. Thomas, Field induced spin reorientation in orthoferrites $DyFeO_3$, $HoFeO_3$ and $ErFeO_3$, J. Magn. Magn. Mater. **15–18**, 557 (1980).

[22] G. F. Herrmann, Magnetic resonances and susceptibility in orthoferrites, Phys. Rev. **133**, A1334 (1964).

[23] C. W. Searle and S. T. Wang, Magnetic-resonance properties of pure and titanium-doped hematite, J. Appl. Phys. **39**, 1025 (1968).

[24] S. Nakatsuji, N. Kiyohara, and T. Higo, Large anomalous Hall effect in a non-collinear antiferromagnet at room temperature, Nature (London) **527**, 212 (2015).

[25] A. Moskvin, Dzyaloshinskii-Moriya coupling in 3d insulators, Condens. Matter **4**, 4 (2019).

[26] R. Lebrun, A. Ross, O. Gomonay, S. A. Bender, L. Baldrati, F. Kronast, A. Qaiumzadeh, J. Sinova, A. Brataas, R. A. Duine, and M. Kläui, Anisotropies and magnetic phase transitions in insulating antiferromagnets determined by a spin-Hall magnetoresistance probe, Commun. Phys. **2**, 50 (2019).

[27] O. R. Sulymenko, O. V. Prokopenko, V. S. Tiberkevich, A. N. Slavin, B. A. Ivanov, and R. S. Khymyn, Terahertz-Frequency Spin Hall Auto-Oscillator Based on a Canted Antiferromagnet, Phys. Rev. Applied **8**, 064007 (2017).

[28] H. J. Fink, Resonance line shapes of weak ferromagnets of the α-Fe_2O_3 and NiF_2 type, Phys. Rev. **133**, A1322 (1964).

[29] R. Lebrun, A. Ross, O. Gomonay, V. Baltz, U. Ebels, A. L. Barra, A. Qaiumzadeh, A. Brataas, J. Sinova, and M. Kläui, Long-distance spin-transport across the Morin phase transition up to room temperature in the ultra-low damping α-Fe_2O_3 antiferromagnet, Nat. Commun. **11**, 6332 (2020).

[30] J. Shim, S.-J. Kim, S. K. Kim, and K.-J. Lee, Enhanced Magnon-Photon Coupling at the Angular Momentum Compensation Point of Ferrimagnets, Phys. Rev. Lett. **125**, 027205 (2020).

[31] See Supplemental Material at http://link.aps.org/supplemental/10.1103/PhysRevLett.126.187201 for the theoretical modeling of the magnetization dynamics of canted antiferromagnets and their spin-pumping response, and experimental data on the resonance and spin-pumping response of the easy-axis antiferromagnet Cr_2O_3 and in the easy-axis phase of α-Fe_2O_3, which includes Ref. [32].

[32] R. Lebrun, A. Ross, S. A. Bender, A. Qaiumzadeh, L. Baldrati, J. Cramer, A. Brataas, R. A. Duine, and M. Kläui, Tunable long-distance spin transport in a crystalline antiferromagnetic iron oxide, Nature (London) **561**, 222 (2018).

[33] R. Cheng, D. Xiao, and A. Brataas, Terahertz Antiferromagnetic Spin Hall Nano-Oscillator, Phys. Rev. Lett. **116**, 207603 (2016).

[34] A. G. Gurevich and G. A. Melkov, *Magnetization Oscillations and Waves* (CRC Press, Boca Raton, 1996).

[35] A. V. Kimel, C. D. Stanciu, P. A. Usachev, R. V. Pisarev, V. N. Gridnev, A. Kirilyuk, and Th. Rasing, Optical excitation of antiferromagnetic resonance in $TmFeO_3$, Phys. Rev. B **74**, 060403(R) (2006).

[36] J. C. Burgiel and M. W. P. Strandberg, Antiferromagnetic resonance linewidth in MnF_2 near the transition temperature, J. Appl. Phys. **35**, 852 (1964).

[37] L. Li, Q. Shi, M. Mino, H. Yamazaki, and I. Yamada, Experimental observation of the antiferromagnetic resonance linewidth in $KCuF_3$, J. Phys. Condens. Matter **17**, 2749 (2005).

[38] Y. Mukai, H. Hirori, T. Yamamoto, H. Kageyama, and K. Tanaka, Antiferromagnetic resonance excitation by terahertz magnetic field resonantly enhanced with split ring resonator, Appl. Phys. Lett. **105**, 022410 (2014).

[39] T. Moriyama, K. Hayashi, K. Yamada, M. Shima, Y. Ohya, and T. Ono, Tailoring THz antiferromagnetic resonance of NiO by cation substitution, Phys. Rev. Mater. **4**, 074402 (2020).

[40] A. O. Kiselev, V. I. Ozhogin, and V. L. Preobrazhenskii, Bistability of above-threshold oscillations of parametric magnetoelastic waves in hematite, JETP Lett. **52**, 82 (1990).

[41] H. Watanabe, T. Kurihara, T. Kato, K. Yamaguchi, and T. Suemoto, Observation of long-lived coherent spin precession in orthoferrite $ErFeO_3$ induced by terahertz magnetic fields, Appl. Phys. Lett. **111**, 092401 (2017).

[42] A. A. Mukhin, A. N. Lobanov, M. Goiran, J. Leotin, and A. A. Volkov, Quasioptical study of antiferromagnetic resonance in $YFeO_3$ at submillimeter wavelength under high pulsed magnetic fields, J. Magn. Reson. **195**, 60 (2008).

[43] J.-C. Rojas-Sánchez, N. Reyren, P. Laczkowski, W. Savero, J.-P. Attané, C. Deranlot, M. Jamet, J.-M. George, L. Vila, and H. Jaffrès, Spin Pumping and Inverse Spin Hall Effect in Platinum: The Essential Role of Spin-Memory Loss at Metallic Interfaces, Phys. Rev. Lett. **112**, 106602 (2014).

[44] O. d'Allivy Kelly, A. Anane, R. Bernard, J. B. Youssef, C. Hahn, A. H. Molpeceres, C. Carrétéro, E. Jacquet, C. Deranlot, P. Bortolotti, R. Lebourgeois, J.-C. Mage, G. de Loubens, O. Klein, V. Cros, and A. Fert, Inverse spin Hall effect in nanometer-thick yttrium iron garnet/Pt system, Appl. Phys. Lett. **103**, 082408 (2013).

[45] A. Ross, R. Lebrun, O. Gomonay, D. A. Grave, A. Kay, L. Baldrati, S. Becker, A. Qaiumzadeh, C. Ulloa, G. Jakob, F. Kronast, J. Sinova, R. Duine, A. Brataas, A. Rothschild, and M. Kläui, Propagation length of antiferromagnetic magnons governed by domain configurations, Nano Lett. **20**, 306 (2020).

[46] V. M. Judin, A. B. Sherman, and I. E. Myl'nikova, Magnetic properties of $YFeO_3$, Phys. Lett. **22**, 554 (1966).

[47] Z. Jin, Z. Mics, G. Ma, Z. Cheng, M. Bonn, and D. Turchinovich, Single-pulse terahertz coherent control of spin resonance in the canted antiferromagnet $YFeO_3$, mediated by dielectric anisotropy, Phys. Rev. B **87**, 094422 (2013).

[48] K. P. Belov, A. M. Kadomtseva, N. M. Kovtun, V. N. Derkachenko, V. N. Melov, and V. A. Khokhlov, On the character of phase transitions in $ErFeO_3$, Phys. Status Solidi A **36**, 415 (1976).

[49] R. M. White, R. J. Nemanich, and C. Herring, Light scattering from magnetic excitations in orthoferrites, Phys. Rev. B **25**, 1822 (1982).

[50] M. Eibschütz, S. Shtrikman, and D. Treves, Mossbauer studies of Fe_{57} in orthoferrites, Phys. Rev. **156**, 562 (1967).

[51] J. Han, P. Zhang, Z. Bi, Y. Fan, T. S. Safi, J. Xiang, J. Finley, L. Fu, R. Cheng, and L. Liu, Birefringence-like spin transport via linearly polarized antiferromagnetic magnons, Nat. Nanotechnol. **15**, 563 (2020).

[52] Y. S. Chen, J. G. Lin, S. Y. Huang, and C. L. Chien, Incoherent spin pumping from YIG single crystals, Phys. Rev. B **99**, 220402(R) (2019).

[53] M. Schreier, G. E. W. Bauer, V. I. Vasyuchka, J. Flipse, K. Uchida, J. Lotze, V. Lauer, A. V. Chumak, A. A. Serga, S. Daimon, T. Kikkawa, E. Saitoh, B. J. van Wees, B. Hillebrands, R. Gross, and S. T. B. Goennenwein, Sign of inverse spin Hall voltages generated by ferromagnetic resonance and temperature gradients in yttrium iron garnet platinum bilayers, J. Phys. D **48**, 025001 (2015).

[54] M. Dąbrowski, T. Nakano, D. M. Burn, A. Frisk, D. G. Newman, C. Klewe, Q. Li, M. Yang, P. Shafer, E. Arenholz, T. Hesjedal, G. van der Laan, Z. Q. Qiu, and R. J. Hicken, Coherent Transfer of Spin Angular Momentum by Evanescent Spin Waves within Antiferromagnetic NiO, Phys. Rev. Lett. **124**, 217201 (2020).

[55] Q. Li, M. Yang, C. Klewe, P. Shafer, A. T. N'Diaye, D. Hou, T. Y. Wang, N. Gao, E. Saitoh, C. Hwang, R. J. Hicken, J. Li, E. Arenholz, and Z. Q. Qiu, Coherent ac spin current transmission across an antiferromagnetic CoO insulator, Nat. Commun. **10**, 5265 (2019).

[56] S. M. Rezende, R. L. Rodríguez-Suárez, and A. Azevedo, Theory of the spin Seebeck effect in antiferromagnets, Phys. Rev. B **93**, 014425 (2016).